Theory for Measuring Bivalent Surface Binding Kinetics Using Total Internal Reflection with Fluorescence Photobleaching Recovery

Helen V. Hsieh* and Nancy L. Thompson
Department of Chemistry, University of North Carolina, Chapel Hill, North Carolina 27599-3290 USA

ABSTRACT   Total internal reflection with fluorescence photobleaching recovery (TIR-FPR) is a method for experimentally examining coupled diffusion and reaction kinetics at surfaces. In a previous work (Thompson et al. 1981. *Biophys. J.* 33:435–454), a theoretical basis for interpreting TIR-FPR data was described for monovalent ligands that undergo a reversible reaction with monovalent surface sites in a single step. Here, the theory for TIR-FPR has been extended to two different surface binding mechanisms that involve sequential, bivalent surface attachment. Methods for obtaining the intrinsic surface association and dissociation kinetic rates from measured fluorescence photobleaching recovery curves are described. The new theory should be applicable to the association of bivalent protein ligands such as antibodies with supported planar model membranes.

GLOSSARY

A	concentration of molecules in solution
B	density of unoccupied surface binding sites
b	as a subscript of A, U, or V, denotes concentration of bleached molecules
C_i	constants that depend on η and Λ
D	surface diffusion coefficient ($D \equiv D_U = D_V$)
$D_{A,U,V}$	diffusion coefficients of A, U, or V
eq	as a subscript of A, U, or V, denotes concentration at equilibrium
$F(t)$	fluorescence at time t
$F(0)$	fluorescence at time $t = 0$
$F(-)$	fluorescence before the bleach pulse
f	fraction of surface bound molecules in U form
g	amplitude of α_1 term in $H(\theta, t)$ (in the reaction limit)
$G(t)$	monotonically decreasing function that describes the TIR-FPR recovery curve
h	overall length of an evanescent intensity pattern along x
$H(\mathbf{q}, t)$	function describing U and V as a function of q and t
I_0	intensity at $r = (0, 0)$
$I(\mathbf{r})$	evanescent illumination profile
$I_{0,1}(\eta\Lambda)$	modified Bessel functions
K_1	equilibrium association constant, first step of mechanisms I and II
K_2	equilibrium association constant, second step of mechanism I
K_3	equilibrium association constant, second step of mechanism II
K_a	apparent association constant in mechanism I
k_i	kinetic rate constants
k_b	kinetic reverse rate in second step of mechanisms I and II

k_f	kinetic forward rate in second step of mechanisms I and II
k_{obs}	inverse of time when $G(t) = e^{-1}$
k_{rx}	inverse of time when the reaction-limited form of $G(t) = e^{-1}$
L^{-1}	inverse Laplace transform
ℓ	characteristic distance of the evanescently illuminated area
N	maximum surface density of bound molecules
n_1	refractive index of denser medium
n_2	refractive index of rarer medium
P	period of an evanescent interference pattern
Q	product of the efficiencies of excitation light absorption and fluorescence emission and detection
q	Fourier transform variable (from $\mathbf{r}$)
R	bulk diffusion rate
R_0	bulk diffusion rate for monovalent binding and $A_{eq} = 0$
$\mathbf{r}$	vector in the sample plane (x, y)
s	semi-minor $1/e^2$ width for a Gaussian-shaped, elliptical evanescent intensity
t	time
U	initial membrane-bound complex formed as A and B bind
u	as a subscript of A, U, or V, denotes unbleached molecules
V	final membrane-bound complex formed as A and B bind
x	intersection of the incidence and sample planes
$X(q, \alpha)$	numerator of function defining $H(\mathbf{q}, t)$
y	with x, defines the sample plane
$Y(q, \alpha)$	denominator of function defining $H(\mathbf{q}, t)$
z	normal to the sample plane
α	Laplace transform variable ($\alpha = \omega + D_A q^2$)
$\sqrt{\alpha_i}$	roots of $Y(q, \alpha)$
β	fractional bleach
γ	constant term related to the eccentricity of the ellipse for a Gaussian-shaped evanescent intensity profile
η	parameter that describes the depth of bleach
θ	spatial periodicity of an evanescent interference pattern
κ	constant related to bleaching depth
Λ	visibility of a periodic evanescent interference pattern
ρ	sum of rate constants ($\rho = k_{-1} + k_b + k_f$)
ϕ	incidence angle in TIR (measured from normal to interface)

ϕ_c critical angle in TIR ($\phi_c = \sin^{-1}(n_2/n_1)$)

ω Laplace transform variable (from t)

INTRODUCTION

The rates of biochemical reactions that occur between ligands in solution and receptors on cell membranes may depend in a complex manner on a number of factors other than the intrinsic receptor-ligand kinetic rates. For example, previous theoretical considerations have demonstrated that receptor-ligand kinetics can depend on the ligand diffusion coefficient in solution and on the ligand solution concentration. In addition, receptor-ligand kinetics may depend on the receptor density and diffusion coefficient if the ligand is bivalent or multivalent for the receptor, or if the ligand induces receptor clustering and the association and/or dissociation kinetic rates depend on the state of receptor oligomerization (Berg and Purcell, 1977; Dembo and Goldstein, 1978; Kaufman and Jain, 1991; Erickson et al., 1987; Goldstein et al., 1989).

One method for experimentally examining coupled diffusion and reaction kinetics at surfaces is to use total internal reflection with fluorescence photobleaching recovery (TIR-FPR) (Thompson et al., 1981). In this technique, fluorescent ligands that are reversibly adsorbed to a liquid/solid interface are illuminated with the evanescent field created by a totally internally reflected laser beam (Fig. 1 *a*). Adsorbed molecules are bleached with an intense laser pulse, and subsequent fluorescent recovery occurs as bleached molecules exchange with unbleached molecules by surface association and dissociation or by diffusion along the surface (Fig. 1 *b*). In general, TIR-FPR recovery curves depend on the surface binding mechanism and its intrinsic rate constants, the bulk and surface diffusion coefficients, the surface site densities, and the shape of the evanescently illuminated area.

Previous experimental work has demonstrated the applicability of TIR-FPR to the adsorption of proteins on quartz or polymer-coated quartz (Burghardt and Axelrod, 1981; Tilton et al., 1990a; Tilton et al., 1990b; Schmidt et al., 1990). TIR-FPR has also been used very recently to examine the kinetics of surface reactions that have biological specificity, i.e., anti-dinitrophenyl Fabs at phospholipid Langmuir-Blodgett films containing dinitrophenyl-conjugated phospholipids (Pisarchick et al., 1992), bovine prothrombin fragment 1 at supported planar phospholipid membranes containing phosphatidylserine (Pearce et al., 1992; Pearce et al., 1993), and antibodies at planar membranes containing antibody receptors (Hsieh and Thompson, manuscript in preparation). In principle, TIR-FPR should be applicable to a large variety of protein ligands at substrate-supported models of cell membranes. This technique has also recently been used to examine the binding kinetics of epidermal growth factor to its receptor on human epidermoid cells adsorbed to quartz (Hellen and Axelrod, 1991).

A theoretical basis for interpreting TIR-FPR recovery curves has previously been developed (Thompson et al., 1981). This previous work describes how one can obtain a measure of the dissociation rate constant and/or surface dif-
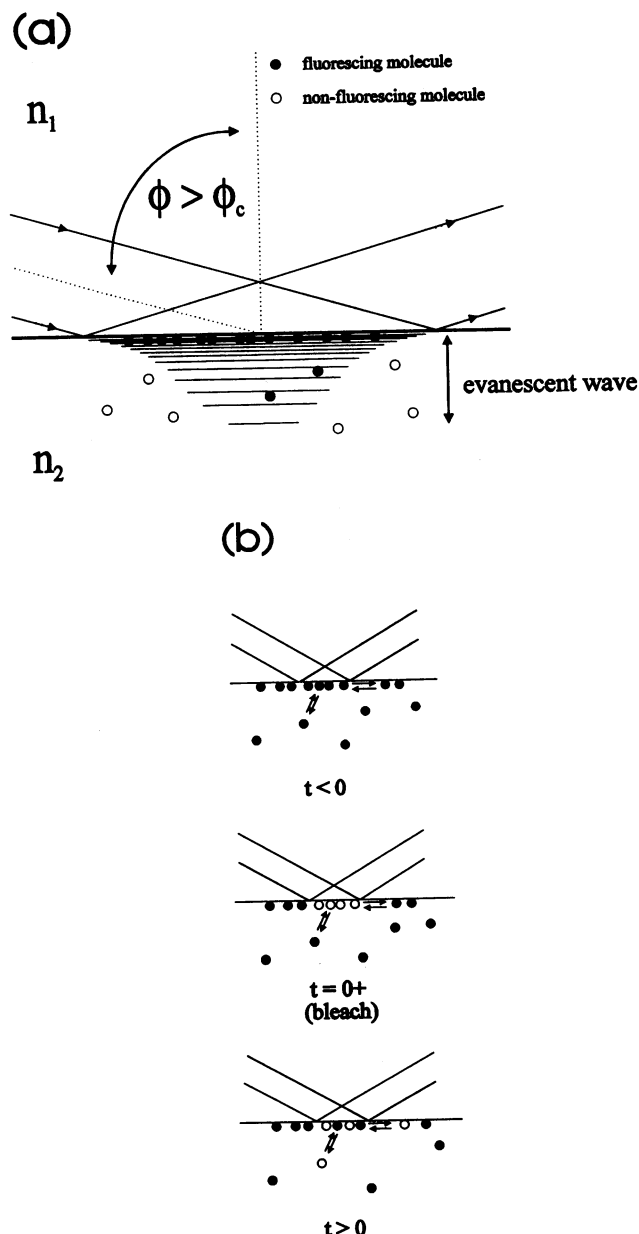

FIGURE 1 Conceptual basis for TIR-FPR. (*a*) Light traveling through a medium of higher refractive index (n_1) encounters a medium of lower refractive index (n_2) at an angle ϕ, which is greater than the critical angle $\phi_c = \sin^{-1}(n_2/n_1)$, and undergoes total internal reflection at the interface. The internal reflection generates a thin evanescent wave which excites fluorescent molecules that are close to the interface. (*b*) In TIR-FPR, the exchange of bleached, surface-bound, fluorescent molecules with unbleached molecules from solution or the surrounding non-illuminated surface area is investigated by monitoring the evanescently excited fluorescence intensity before and after an intense pulse of light as a function of time.

fusion coefficient for monovalent ligands that undergo a reversible reaction with monovalent surface sites in a single step. However, the four biologically specific model systems that have thus far been examined with TIR-FPR exhibit more complex surface reaction mechanisms (Pisarchick et al., 1992; Pearce et al., 1992; Pearce et al., 1993; Hellen and Axelrod, 1991; Hsieh and Thompson, manuscript in preparation). Also, receptor-ligand kinetics measured by other

methods often demonstrate multi-step mechanisms (Müller et al., 1993; Ortega et al., 1991). In this paper, we develop a theoretical basis for TIR-FPR using two different surface binding mechanisms in which the ligand is bivalent for the surface. The results should be applicable to the binding of bivalent protein ligands, such as antibodies, to planar model membranes.

MODELS FOR BIVALENT SURFACE BINDING

Two different models for bivalent surface binding are considered (Fig. 2). Here, A denotes ligands freely diffusing in solution, B denotes free surface binding sites, and U and V are surface-bound complexes. In mechanism I, one segment of molecule A is bound to one binding site B to form a surface complex U. The monovalently bound complex U then isomerizes to a bivalently bound state, denoted by V. In mechanism II, the formation of the monovalently bound complex U is identical to the first step in mechanism I. In the second step, the complex U combines with an additional binding site B to form a bivalently bound complex V. The two mecha-

(a)

(b)
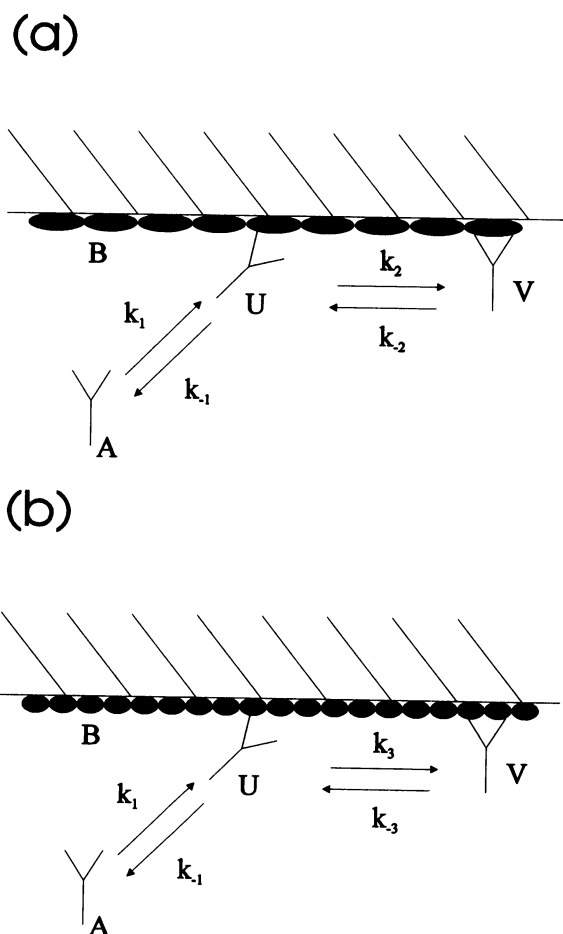

FIGURE 2   Mechanisms for bivalent surface binding. (a) In mechanism I, molecules A are bound to single binding sites B; the surface-bound complexes then isomerize between monovalently (U) and bivalently (V) bound states. (b) In mechanism II, molecules A may be surface bound by attaching to either one (U) or two (V) binding sites B.

nisms differ in that the formation of V consumes only one binding site B in the first mechanism, whereas two binding sites B are consumed in the second. Both models have been used to describe the association of bivalent ligands with surfaces (Pisarchick and Thompson, 1990).

The relationships between the equilibrium association constants (K_i), the equilibrium concentrations (denoted by the subscript eq), and the kinetic rate constants (k_i) are

$$K_1 = \frac{U_{eq}}{A_{eq}B_{eq}} = \frac{k_1}{k_{-1}}$$

$$K_2 = \frac{V_{eq}}{U_{eq}} = \frac{k_2}{k_{-2}} \qquad (1.1)$$

$$K_3 = \frac{V_{eq}}{U_{eq}B_{eq}} = \frac{k_3}{k_{-3}}$$

The shapes of the equilibrium binding curves for mechanisms I and II have been described previously (Pisarchick and Thompson, 1990). For mechanism I, the surface density of bound molecules ($U_{eq} + V_{eq}$) as a function of the solution concentration (A_{eq}) has the following shape

$$U_{eq} + V_{eq} = \frac{K_a A_{eq} N}{1 + K_a A_{eq}} \qquad (1.2)$$

where $N = B_{eq} + U_{eq} + V_{eq}$ is the maximum surface density of bound molecules and

$$K_a = K_1(1 + K_2) \qquad (1.3)$$

Eq. 1.2 has the shape of a conventional saturation curve with an apparent association constant, K_a. A measure of $U_{eq} + V_{eq}$ as a function of A_{eq} will give a value for K_a but will not give values for both K_1 and K_2. For mechanism II, the surface density of bound molecules ($U_{eq} + V_{eq}$) as a function of the solution concentration (A_{eq}) has a different shape, i.e.,

$$U_{eq} + V_{eq} = [1 + 4K_1 A_{eq} K_3 N - (K_1 A_{eq})^2 + (K_1 A_{eq} - 1)$$
$$\cdot \sqrt{(1 + K_1 A_{eq})^2 + 8K_1 A_{eq} K_3 N}]$$
$$\div 8K_1 A_{eq} K_3 \qquad (1.4)$$

where $N = B_{eq} + U_{eq} + 2V_{eq}$ is the density of bound molecules at saturation. Theoretically, measuring $U_{eq} + V_{eq}$ as a function of A_{eq} and N will yield independent measures of K_1 and K_3. The surface is half saturated when $A_{eq} = K_1^{-1}$. For monovalent binding,

$$U_{eq} = \frac{K_1 A_{eq} N}{1 + K_1 A_{eq}} \qquad (1.5)$$

where $N = B_{eq} + U_{eq}$. The binding curve for mechanism I (Eq. 1.2) reduces to this expression when $K_2 \rightarrow 0$. The binding curve for mechanism II (Eq. 1.4) reduces to Eq. 1.5 when $K_3 \rightarrow 0$.

GENERAL SOLUTION FOR THE TIR-FPR RECOVERY CURVE

It is convenient to normalize the TIR-FPR recovery curve, $F(t)$, by the prebleach value, $F(-)$, and to write the nor-

malized function in terms of the fractional bleach, β, and a function $G(t)$:

$$\frac{F(t)}{F(-)} = 1 - \beta G(t)$$

$$\beta = \frac{F(-) - F(0)}{F(-)} \tag{2.1}$$

$$G(t) = \frac{F(-) - F(t)}{F(-) - F(0)}$$

$G(t)$ describes the rate and shape of the fluorescence recovery. This function is unitless, monotonically decreasing, equals one at time 0, and equals 0 at infinite time. The quantities $G(t)$, β, and $F(-)$ completely describe the TIR-FPR fluorescence recovery curve $F(t)$ (Fig. 3).

As shown in the Appendix, $F(t)$ is (and therefore $G(t)$, β, and $F(-)$ are) determined by the densities of the two surface-bound species as a function of time and space, by the shape and intensity of the evanescent illumination, $I(\mathbf{r})$, and by a constant that defines the bleaching depth, κ. Here, $\mathbf{r} = (x, y)$ is a vector that lies in the sample plane (i.e., the plane where total internal reflection occurs), $\mathbf{q}$ is a Fourier transform variable (from $\mathbf{r}$), and

$$G(t) = \frac{\int d^2r \int d^2r' \int d^2q I(\mathbf{r})[1 - e^{-\kappa I(r')}]e^{i\mathbf{q}\cdot(\mathbf{r}-\mathbf{r}')}H(\mathbf{q}, t)}{4\pi^2 \int d^2r I(\mathbf{r})[1 - e^{-\kappa I(\mathbf{r})}]} \tag{2.2}$$

where

$$H(\mathbf{q}, t) = e^{-q^2 D_A t} L_{\alpha \to t}^{-1}\left[\frac{X(q, \alpha)}{Y(q, \alpha)}\right] \tag{2.3}$$

$$X(q, \alpha) = \left[\sqrt{\alpha} + \frac{fk_{-1}}{\sqrt{R}}\right][\alpha + k_f + k_b + (1 - f)k_{-1}$$

$$+ \{(1 - f)D_U + fD_V - D_A\}q^2] - \frac{k_{-1}^2 f(1 - f)}{\sqrt{R}} \tag{2.4}$$

bleach
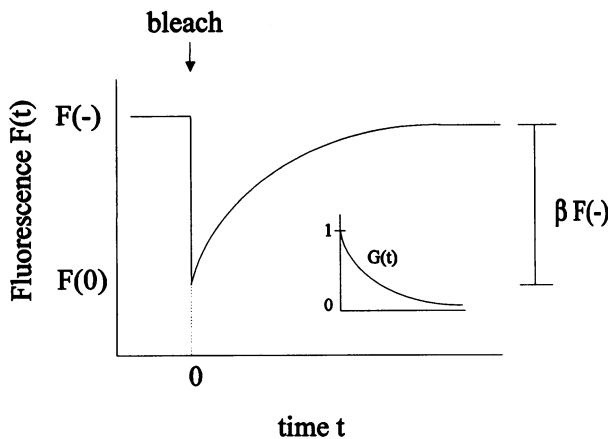

FIGURE 3 Relationship between $F(t)$, $F(-)$, $G(t)$ and β. Shown is a schematic of a TIR-FPR fluorescence recovery curve. $F(-)$ is the fluorescence before to the bleach pulse, $F(0)$ is the fluorescence at the bleach pulse, β is the depth of the bleach, and the function $G(t)$ describes the rate and shape of the fluorescence recovery.

$Y(q, \alpha)$

$$= \left[\sqrt{\alpha} + \frac{fk_{-1}}{\sqrt{R}}\right][\{\alpha + k_b + (D_V - D_A)q^2\}$$

$$\cdot \{\alpha + k_f + k_{-1} + (D_U - D_A)q^2\} - k_f k_b] \tag{2.5}$$

$$- \frac{k_{-1}^2 f}{\sqrt{R}}[\alpha + k_b + (D_V - D_A)q^2]$$

$$k_f = \left\{ \begin{array}{ll} k_2 & \text{(mechanism I)} \\ k_3 B_{eq} & \text{(mechanism II)} \end{array} \right.$$

$$k_b = \left\{ \begin{array}{ll} k_{-2} & \text{(mechanism I)} \\ k_{-3} & \text{(mechanism II)} \end{array} \right. \tag{2.6}$$

$$R = D_A\left(\frac{A_{eq}}{U_{eq} + V_{eq}}\right)^2 \tag{2.7}$$

$L_{\alpha \to t}^{-1}$ denotes an inverse Laplace transform, $f = U_{eq}/(U_{eq} + V_{eq}) = k_b/(k_b + k_f)$ is the fraction of membrane-bound molecules in the initial state of attachment, D_A is the solution diffusion coefficient, and D_U and D_V are the surface diffusion coefficients of the two bound species. The method of partial fractions may be used to carry out the inverse Laplace transform in Eq. 2.3. $G(t)$ is given in general by Eq. 2.2 with

$$H(q, t) = \sum_{i=1}^{5}[X(q, \alpha_i)\sqrt{\alpha_i}\exp[(\alpha_i - D_A q^2)t]\text{erfc}(-\sqrt{\alpha_i}t)]$$

$$\div [(\sqrt{\alpha_i} - \sqrt{\alpha_j})(\sqrt{\alpha_i} - \sqrt{\alpha_k}) \tag{2.8}$$

$$\cdot (\sqrt{\alpha_i} - \sqrt{\alpha_l})(\sqrt{\alpha_i} - \sqrt{\alpha_m})]$$

where $X(q, \alpha_i)$ is given by Eq. 2.4 evaluated at $\sqrt{\alpha} = \sqrt{\alpha_i}$, $\sqrt{\alpha_i}$ (for $i = 1$ to 5) are the five roots of Eq. 2.5, and $\sqrt{\alpha_j}$, $\sqrt{\alpha_k}$, $\sqrt{\alpha_l}$, and $\sqrt{\alpha_m}$ are the four roots of Eq. 2.5 that are different from $\sqrt{\alpha_i}$.

CHARACTERISTIC RATES

As shown in Eqs. 2.2–2.7, $G(t)$ depends in general on seven characteristic rates. Two of these rates (k_{-1} and k_b) are dissociation rate constants that are intrinsic to the binding mechanisms. A third rate (k_f) differs for the two mechanisms. In mechanism I, $k_f = k_2$ is an intrinsic association constant; in mechanism II, $k_f = k_3 B_{eq}$ depends on the density of free surface sites (i.e., on the solution concentration). Here (Pisarchick and Thompson, 1990)

$$B_{eq} = \frac{-(1 + K_1 A_{eq}) + \sqrt{(1 + K_1 A_{eq})^2 + 8K_1 A_{eq} K_3 N}}{4K_1 A_{eq} K_3} \tag{3.1}$$

When $A_{eq} \to 0$ (far from saturation), the density of free sites is approximately equal to the maximum density of bound molecules and $k_f \to k_3 N$. When $A_{eq} \to \infty$ (at saturation), $B_{eq} \to 0$ and $k_f \to 0$. The dependence of k_f on the solution concentration is shown in Fig. 4 a.

Three of the seven characteristic rates that determine $G(t)$ are transport rates which describe diffusion through a characteristic distance, ℓ, of the evanescent area. One rate depends on the diffusion coefficient of molecules in
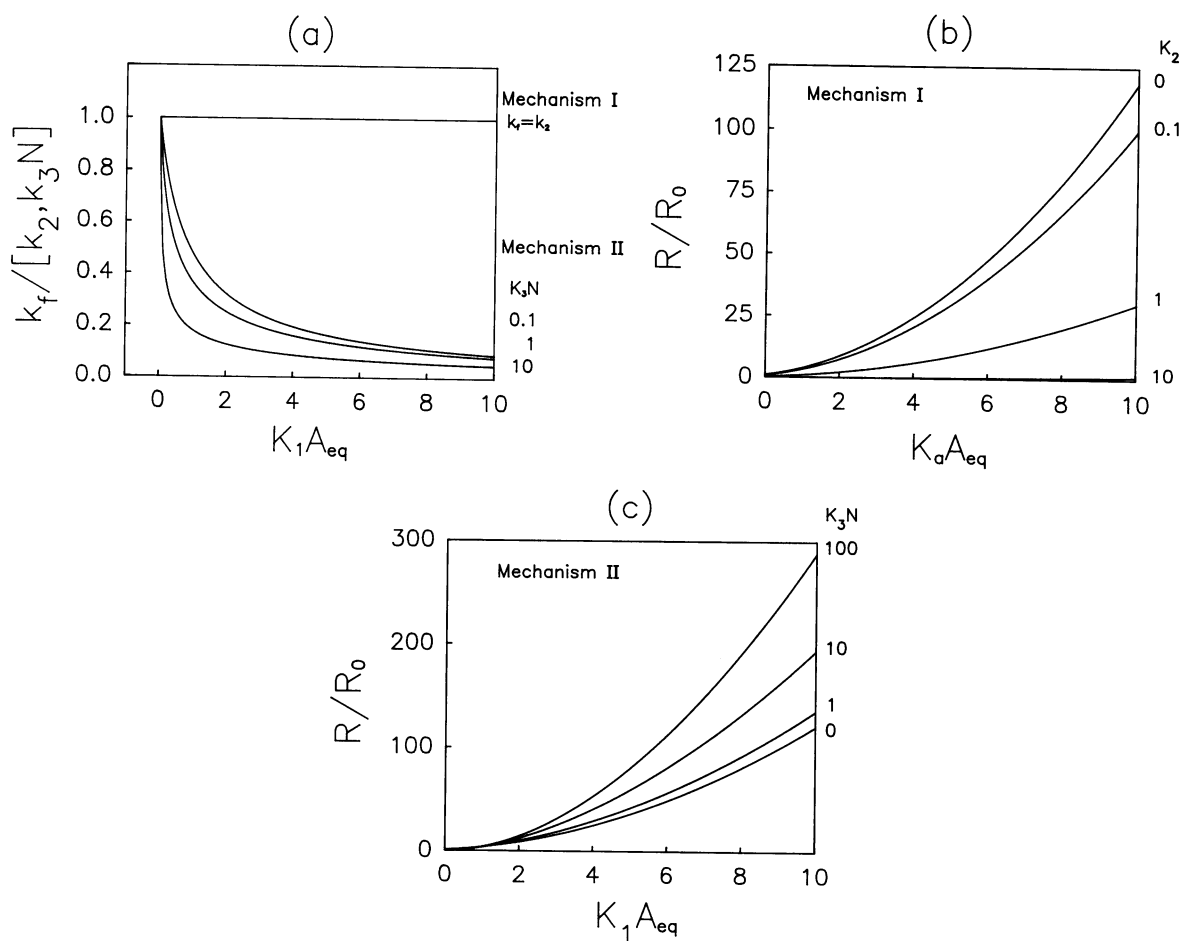
FIGURE 4   Rates k_f and R as a function of the solution concentration A_{eq}. (a) For mechanism I, $k_f = k_2$ and does not depend on A_{eq}. For mechanism II, k_f ranges from k_3N to 0 with increasing values of K_1A_{eq}. Curves were calculated using Eqs. 2.6 and 3.1 and are shown for $K_3N = 0.1$, 1, and 10. (b) For mechanism I, R/R_0 increases with K_aA_{eq} and also depends on K_2. Curves were calculated using Eq. 3.4 and are shown for $K_2 = 0, 0.1, 1,$ and 10. (c) For mechanism II, R/R_0 increases with K_1A_{eq} and also depends on K_3N. Curves were calculated using Eq. 3.5 and are shown for $K_3N = 0, 1, 10,$ and 100.

solution (D_A/ℓ^2) and the other two rates depend on the diffusion coefficients of the two bound species $(D_U/\ell^2$ and $D_V/\ell^2)$.

The last of the seven rates, R (Eq. 2.7), describes diffusion in solution through a characteristic distance $(U_{eq} + V_{eq})/A_{eq}$. This distance gives the depth of solution which contains a density of solution molecules equal to the density of surface bound molecules. For monovalent binding,

$$R = R_0(1 + K_1A_{eq})^2 \tag{3.2}$$

where

$$R_0 = \frac{D_A}{(K_1N)^2} \tag{3.3}$$

is the value of R when $A_{eq} = 0$. For mechanism I, R may be written as (see Eq. 1.2)

$$R = R_0\left[\frac{1 + K_aA_{eq}}{1 + K_2}\right]^2 \tag{3.4}$$

The dependence of the diffusion rate R on the value

of K_aA_{eq} is shown in Fig. 4 b for different values of K_2. For mechanism II, the expression for R is more complex. Here (see Eq. 1.4),

$$R = [R_0 64(K_1A_{eq})^4(K_3N)^2]$$
$$\div [1 + 4K_1A_{eq}K_3N - (K_1A_{eq})^2 \tag{3.5}$$
$$+ (K_1A_{eq} - 1)\sqrt{(1 + K_1A_{eq})^2 + 8K_1A_{eq}K_3N}\,]^2$$

The dependence of the diffusion rate R on the value of K_1A_{eq} is shown in Fig. 4 c for different values of K_3N. Eqs. 3.4 and 3.5 reduce to Eq 3.2 when $K_2{\to}0$ or $K_3N{\to}0$, respectively.

SOLUTIONS FOR A LARGE OBSERVATION AREA

General solution

If the evanescently illuminated area is large or if the diffusion coefficients D_A, D_U and D_V are small, then contributions to $G(t)$ that arise from lateral diffusion along the surface or in solution are negligible and the terms in Eqs. 2.3–2.5 that are proportional to q^2 approach 0. Because $H(q, t)$ no longer

depends on q, the integral over q in Eq. 2.2 may be evaluated analytically. This calculation shows that, for a large observation area, $G(t)$ does not depend on the evanescent intensity profile $I(r)$.

Furthermore,

$$G(t) = H(0, t) = L_{\alpha \to t}^{-1}\left[\frac{X(0, \alpha)}{Y(0, \alpha)}\right] \tag{4.1}$$

where (Eqs. 2.4 and 2.5)

$$X(0, \alpha) = \alpha^{3/2} + \frac{fk_{-1}}{\sqrt{R}}\alpha$$
$$+ [k_f + k_b + (1 - f)k_{-1}]\alpha^{1/2} + \frac{k_b k_{-1}}{\sqrt{R}} \tag{4.2}$$

$$Y(0, \alpha) = \sqrt{\alpha}\left[\alpha^2 + \frac{fk_{-1}}{\sqrt{R}}\alpha^{3/2} + (k_f + k_b + k_{-1})\alpha\right.$$
$$\left. + \frac{k_b k_{-1}}{\sqrt{R}}\sqrt{\alpha} + k_b k_{-1}\right] \tag{4.3}$$

The method of partial fractions may be used to derive the following general expression for $G(t)$ when the evanescently illuminated area is large:

$$G(t) = \sum_{i=1}^{4} \frac{X(0, \alpha_i)e^{\alpha_i t}\text{erfc}(-\sqrt{\alpha_i}t)}{(\sqrt{\alpha_i} - \sqrt{\alpha_j})(\sqrt{\alpha_i} - \sqrt{\alpha_k})(\sqrt{\alpha_i} - \sqrt{\alpha_l})} \tag{4.4}$$

where the $\sqrt{\alpha}$ are the four non-zero roots of Eq. 4.3, $X(0, \alpha i)$ is given by Eq. 4.2 evaluated at $\sqrt{\alpha} = \sqrt{\alpha_i}$, and $\sqrt{\alpha_j}$, $\sqrt{\alpha_k}$, and $\sqrt{\alpha_l}$ are the three roots of Eq.4.3 that are different from $\sqrt{\alpha_i}$.

Monovalent binding

When $k_f \ll k_b$, all bound molecules are in the initial state of attachment. Here, $f = 1$ and Eqs. 4.1–4.3 reduce to

$$G(t) = L_{\alpha \to t}^{-1}\left[\frac{\sqrt{\alpha} + (k_{-1}/\sqrt{R})}{\sqrt{\alpha}(\alpha + (k_{-1}/\sqrt{R})\sqrt{\alpha} + k_{-1})}\right] \tag{4.5}$$

Eq. 4.5 yields the previously derived expression for large observation areas and monovalent binding (Thompson et al., 1981):

$$G(t) = [\sqrt{\alpha_1}\exp(\alpha_2 t)\text{erfc}(-\sqrt{\alpha_2}t)$$
$$- \sqrt{\alpha_2}\exp(\alpha_1 t)\text{erfc}(-\sqrt{\alpha_1}t)] \tag{4.6}$$
$$\div [\sqrt{\alpha_1} - \sqrt{\alpha_2}]$$

where

$$\sqrt{\alpha_{1,2}} = -\frac{1}{2}\left[\frac{k_{-1}}{\sqrt{R}} \pm \sqrt{\frac{k_{-1}^2}{R} - 4k_{-1}}\right] \tag{4.7}$$

When $k_{-1} \ll R$, the recovery curve is reaction-limited (i.e., $G(t)$ depends only on the intrinsic dissociation rate k_{-1}), and
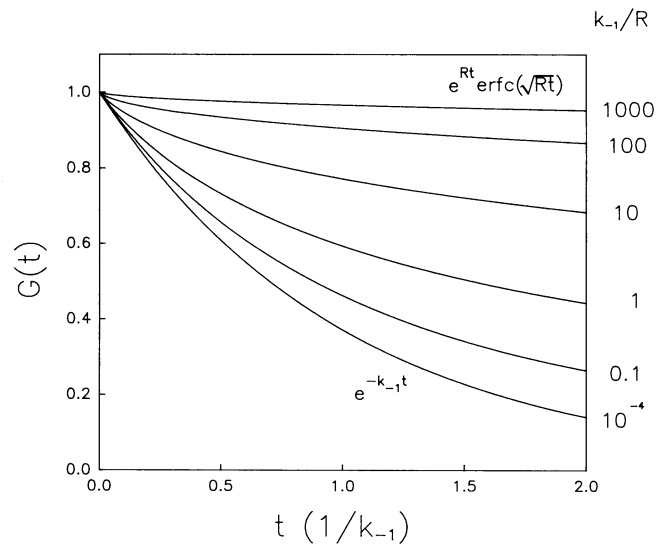

FIGURE 5 $G(t)$ for a large observation area and monovalent binding. $G(t)$ is shown as calculated from Eq. 4.6. When $k_{-1} \ll R$, $G(t)$ is reaction-limited (Eq. 4.8). When $k_{-1} \gg R$, $G(t)$ is diffusion-limited (Eq. 4.9).

Eqs. 4.6 and 4.7 reduce to

$$G(t) = \exp(-k_{-1}t) \tag{4.8}$$

When $R \ll k_{-1}$, the recovery curve is diffusion-limited (i.e., $G(t)$ depends only on the solution diffusion rate R), and Eqs. 4.6 and 4.7 reduce to

$$G(t) = \exp(Rt)\text{erfc}(\sqrt{Rt}) \tag{4.9}$$

Note: this equation contained a sign error in an earlier publication (Thompson et al., 1981). These two limiting cases for TIR-FPR recovery curves when the surface binding is monovalent and the illuminated area is large are illustrated in Fig. 5.

Bivalent binding, reaction limit

When $R \to \infty$, Eqs. 4.1–4.3 reduce to

$$G(t) = L_{\alpha \to t}^{-1}\left[\frac{\alpha + k_f + k_b + (1 - f)k_{-1}}{\alpha^2 + (k_f + k_b + k_{-1})\alpha + k_{-1}k_b}\right] \tag{4.10}$$

By using the method of partial fractions, one finds that

$$G(t) = g\exp(-\alpha_1 t) + (1 - g)\exp(-\alpha_2 t) \tag{4.11}$$

where

$$\alpha_{1,2} = \frac{1}{2}[\rho \pm \sqrt{\rho^2 - 4k_{-1}k_b}] \tag{4.12}$$

$$\rho = k_{-1} + k_f + k_b \tag{4.13}$$

$$g = \frac{fk_{-1} - \alpha_2}{\alpha_1 - \alpha_2} \tag{4.14}$$

This result agrees with expressions that have been used

Biophysical Journal

previously to interpret data for three different model biochemical systems (Pisarchick et al., 1992; Pearce et al., 1992; Hsieh and Thompson, manuscript in preparation).

The shape of $G(t)$ (Eqs. 4.11) for different relative values of k_{-1}, k_f and k_b is shown in Fig. 6. There are several conditions for which this equation assumes simpler forms: 1) In a system where $k_f \approx k_b \ll k_{-1}$, significant amounts of both membrane-bound states are occupied, but the conversion between the two states is much slower than membrane dissociation from the initial attached state. In this situation, $\alpha_1 \approx k_{-1}$, $\alpha_2 \approx k_b$, $g \approx f$, and $G(t)$ is biexponential with slow and fast rates that correspond to the two intrinsic dissociation rates. 2) When $k_b \approx k_f \gg k_{-1}$, significant amounts of both membrane-bound states are occupied, and the conversion

between the two states is much faster than membrane dissociation from the initial attached state. Here, $g \approx 0$, and $G(t)$ is monoexponential with rate $\alpha_2 \approx fk_{-1}$. (3) When $k_f \ll k_b$, most of the surface-bound molecules are in the initial state of attachment and $f \approx 1$. In this case, $g \approx 0$, and $G(t)$ is monoexponential with the membrane dissociation rate $\alpha_2 \approx k_{-1}$. (4) When $k_b \ll k_f$, most of the surface bound molecules are in the second state of attachment and $f \approx 0$. Here, $g \approx 0$ and $G(t)$ is monoexponential with rate $\alpha_2 \approx k_{-1}k_b/(k_{-1} + k_f)$. If, in addition, $k_f \ll k_{-1}$, then $\alpha_2 \approx k_b$. Note that for these limiting cases, $G(t)$ is biexponential only when the populations of both bound species are significant, and the intrinsic off rate k_{-1} is faster than the kinetic rates in the second step of mechanisms I and II.

Bivalent binding, diffusion limit

In the diffusion limit $(R \to 0)$, the four roots of Eq. 4.3 are $\sqrt{\alpha_1} \approx -\sqrt{R}$, $\sqrt{\alpha_{2,3}} \approx \pm i(k_f + k_b)^{1/2}$, and $\sqrt{\alpha_4} \approx -fk_{-1}/\sqrt{R}$. The amplitudes of three of the four terms in Eq. 4.4 are approximately 0, the amplitude for the $\sqrt{\alpha_1}$ term is approximately equal to one, and the form of $G(t)$ is identical to that for a monovalent system in the bulk diffusion limit (Eq. 4.9). The recovery curves for this diffusion limit and intermediate cases are illustrated in Fig. 7.

TIR-FPR RECOVERY CURVES FOR FINITE-SIZED EVANESCENT FIELDS

Intensity profiles

In one geometry for TIR-FPR, a laser beam of circular Gaussian intensity profile is totally internally reflected at the planar interface $(z = 0)$, creating a region of evanescent intensity which varies approximately as an elliptical Gaussian in the x–y plane (Burghardt and Axelrod, 1981; Schmidt et al.,
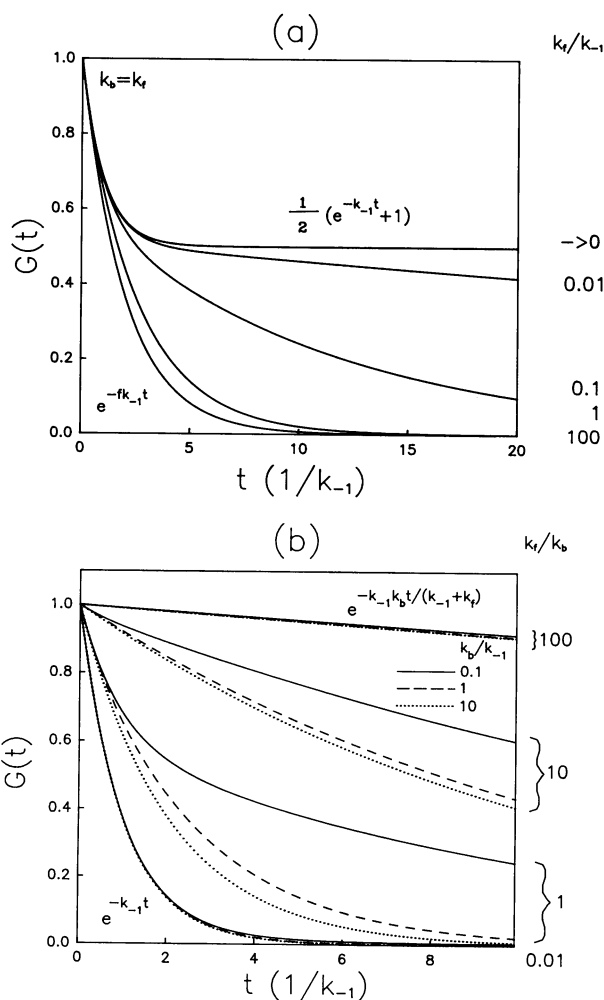

FIGURE 6 $G(t)$ for a large observation area and bivalent binding (reaction limit). $G(t)$ is shown as calculated from Eqs. 4.11–4.14. (a) Here, $k_b = k_f$. As $k_f \to 0$ and $k_b \to 0$, $G(t)$ approaches an upper limit in which the fluorescence recovery is due to the dissociation of U molecules only (first step in mechanisms I and II). $G(t)$ decays only to 0.5 because the V molecules take a very long time to convert to U molecules. As $k_f \to \infty$ and $k_b \to \infty$, $G(t)$ approaches a lower limit in which the shape is exponential with rate fk_{-1}. Note that when $k_f = k_b = k_{-1}$, $G(t)$ is nearly at the lower limit. (b) Here, $k_f \neq k_b$ and $k_b/k_{-1} = 0.1$ (solid), 1 (dash), or 10 (dot). As $k_f/k_b \to \infty$, $G(t)$ is monoexponential with rate $k_{-1}k_b/(k_{-1} + k_f)$. As $k_f/k_b \to 0$, $G(t)$ is monoexponential with rate k_{-1} (see Fig. 5).
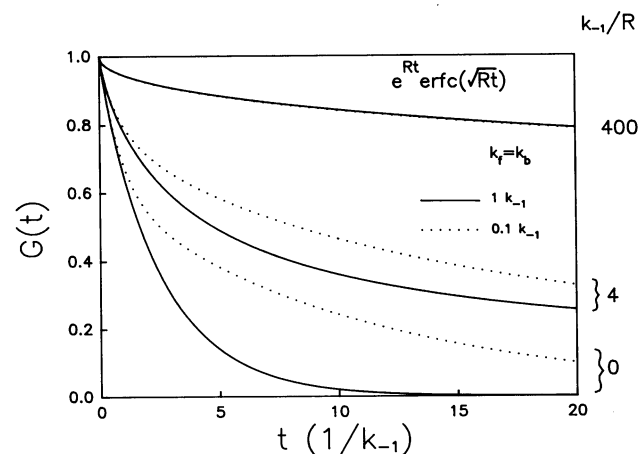

FIGURE 7 $G(t)$ for a large observation area and bivalent binding. $G(t)$ is shown as calculated from Eqs. 4.1–4.4 with $k_f = k_b = k_{-1}$ (solid) and $k_f = k_b = 0.1 k_{-1}$ (dot). As k_{-1}/R approaches 0, $G(t)$ approaches the reaction limit and depends on k_{-1}, k_f, and k_b (see Fig. 6). As k_{-1}/R approaches infinity, $G(t)$ approaches the bulk diffusion limit and depends only on R.

1990; Pisarchick et al., 1992; Pearce et al., 1992; Pearce et al., 1993; Burghardt and Thompson, 1984; Zimmermann et al., 1990; Hsieh and Thompson, manuscript in preparation). Contributions to the fluorescence recovery arising from surface diffusion for this illumination pattern depend on the $1/e^2$- widths of the elliptical Gaussian intensity profile. The functional form for $I(\mathbf{r})$ may be written as (Thompson et al., 1981)

$$I(\mathbf{r}) \approx I_0 e^{-2x^2/(\gamma s)^2} e^{-2y^2/s^2} \qquad (5.1)$$

where I_0 is a constant, s is the semi-minor $1/e^2$ width, the x axis defines the intersection of the incidence plane and the sample plane, and $\gamma > 1$ defines the eccentricity of the ellipse.

In some experimental arrangements, a periodic evanescent interference pattern is created by the collision of two totally internally reflected laser beams (Tilton et al., 1990a; Tilton et al., 1990b; Abney et al., 1992; Weis et al., 1982; Huang, Pearce, and Thompson, manuscript in preparation). Here, contributions to the fluorescence recovery that arise from surface diffusion depend on the period of the interference pattern, P. For this geometry,

$$I(\mathbf{r}) \approx I_0[1 + \Lambda \cos(\theta y)] \qquad (5.2)$$

where $\theta = 2\pi/P$ and the x axis lies in the sample plane and bisects the angle between the two incidence planes. The visibility Λ is related to the contrast of the interference pattern and ranges from 0 to 1 for different experimental conditions (Abney et al., 1992).

General solution

The general solution for $G(t)$ is found by using Eq. 5.1 or 5.2 in Eqs. 2.2–2.7. For the Gaussian-shaped evanescent field, $G(t)$ may be calculated numerically. For an evanescent interference pattern, further analytical calculations are possible. In this case, the denominator of Eq. 2.2 may be evaluated directly (with y ranging from 0 to P and x from $-h$ to h where h is large). In the numerator of Eq. 2.2, the integral over d^2r is an expression that is a sum of terms proportional to $\delta(q_x)\delta(q_y)$, $\delta(q_x)\delta(q_y + \theta)$ and $\delta(q_x)\delta(q_y - \theta)$. By subsequently carrying out the integrals over d^2q and d^2r', one finds the following expression for $G(t)$:

$$G(t) = \frac{C_1 H(0, t) + C_2 H(\theta, t)}{C_1 + C_2} \qquad (5.3)$$

where

$$\begin{aligned} C_1 &= 1 - e^{-\eta} I_0(\eta\Lambda) \\ C_2 &= \Lambda e^{-\eta} I_1(\eta\Lambda) \end{aligned} \qquad (5.4)$$

$H(0, t)$ and $H(\theta, t)$ are given by Eqs. 2.3–2.5 or Eq. 2.8 with $q = 0$ or $q = \theta$, $\eta = \kappa I_0$, and $I_0(\eta\Lambda)$ and $I_1(\eta\Lambda)$ are modified Bessel functions. In the limit of shallow bleaching, Eq. 5.3 simplifies to

$$G(t) = \frac{H(0, t) + (\Lambda^2/2)H(\theta, t)}{1 + \Lambda^2/2} \qquad (\eta \ll 1) \quad (5.5)$$

Monovalent binding

When $k_f \ll k_b$ and all bound molecules are in the initial state of attachment ($f = 1$) (see Eqs. 2.3–2.8)

$$\frac{X(q, \alpha)}{Y(q, \alpha)} \qquad (5.6)$$

$$= \frac{\sqrt{\alpha} + \dfrac{k_{-1}}{\sqrt{R}}}{\left[\sqrt{\alpha} + \dfrac{k_{-1}}{\sqrt{R}}\right][\alpha + k_{-1} + (D_U - D_A)q^2] - \dfrac{k_{-1}^2}{\sqrt{R}}}$$

and

$$H(\mathbf{q}, t) = \sum_{i=1}^{3} \left\{ \frac{\sqrt{\alpha_i}[\sqrt{\alpha_i} + k_{-1}/\sqrt{R}]}{[\sqrt{\alpha_i} - \sqrt{\alpha_j}][\sqrt{\alpha_i} - \sqrt{\alpha_k}]} \right\} \qquad (5.7)$$
$$\cdot \{e^{(\alpha_i - q^2 D_A)t} \mathrm{erfc}(-\sqrt{\alpha_i}t)\}$$

where $\sqrt{\alpha_i}$, $\sqrt{\alpha_j}$, and $\sqrt{\alpha_k}$ are the three roots of the denominator of Eq. 5.6. Using Eqs. 5.1 and 5.7 in Eq. 2.2 gives the shape of the TIR-FPR recovery curve for a Gaussian-shaped evanescent intensity, monovalent surface binding, and surface diffusion. This form for $G(t)$ is equivalent to the previously derived expression (Thompson et al., 1981). By using Eq. 5.7 in Eq. 5.3, the shape of the TIR-FPR recovery curve for a periodic evanescent intensity with monovalent surface binding and surface diffusion may be found.

Of special interest is the reaction-limited case ($k_{-1} \ll R$), where (Eq. 5.6)

$$\frac{X(q, \alpha)}{Y(q, \alpha)} = \frac{1}{\alpha + k_{-1} + (D_U - D_A)q^2} \qquad (5.8)$$

By using the inverse Laplace transform of this expression together with Eq. 5.1 in Eq. 2.2, one finds $G(t)$ for a Gaussian intensity profile in the limit of shallow bleaching ($\eta \ll 1$); $G(t)$ for an evanescent interference pattern may be found using Eqs. 5.3, 5.8, and 2.3 (Table 1, third row). These equations are equivalent to the previously given expressions for monovalent surface binding in the reaction limit (Thompson et al., 1981; Abney et al., 1992). When k_{-1} is small, these equations reduce to previously published forms for pure surface diffusion (Thompson et al., 1981; Abney et al., 1992; Axelrod et al., 1976; Davoust et al., 1982); when D_U is small, the equations reduce to Eq. 4.8.

Bivalent binding

The general solution for $G(t)$ with bivalent binding and surface diffusion is given by Eqs. 2.2, 2.8, and 5.1 (for a Gaussian-shaped evanescent intensity) or by Eqs. 2.8 and 5.3 (for a periodic evanescent intensity). In the reaction limit where $k_{-1} \ll R$, Eqs. 2.4 and 2.5 reduce to

$$\begin{aligned} \frac{X(q, \alpha)}{Y(q, \alpha)} = {}& [\alpha + k_f + k_b + (1 - f)k_{-1} \\ &+ [(1 - f)D_U + fD_V - D_A]q^2] \\ \div {}& \{[\alpha + k_b + (D_V - D_A)q^2] \\ &\cdot [\alpha + k_f + k_{-1} + (D_U - D_A)q^2] - k_f k_b\} \end{aligned} \qquad (5.9)$$

TABLE 1   Limiting cases for a reaction-limited bivalent system with $D \equiv D_V = D_V$

Limiting case	$G(t)$ for Gaussian intensity profile	$G(\theta,t)$ for periodic interference pattern
$k_f \approx k_b \ll k_{-1}$	$\dfrac{f\exp(-k_{-1}t)}{\sqrt{(1 + 4s^{-2}Dt)(1 + 4(\gamma s)^{-2}Dt)}} + \dfrac{(1 - f)\exp(-k_b t)}{\sqrt{(1 + 4s^{-2}Dt)(1 + 4(\gamma s)^{-2}Dt)}}$	$\dfrac{[f\exp(-k_{-1}t) + (1 - f)\exp(-k_b t)][C_1 + C_2\exp(-D\theta^2 t)]}{C_1 + C_2}$
$k_f \approx k_b \gg k_{-1}$	$\exp(-fk_{-1}t)/\sqrt{(1 + 4s^{-2}Dt)(1 + 4(\gamma s)^{-2}Dt)}$	$\exp(-fk_{-1}t)(C_1 + C_2\exp(-D\theta^2 t))/(C_1 + C_2)$
$k_f \ll k_b \;\; (f \approx 1)$	$\exp(-k_{-1}t)/\sqrt{(1 + 4s^{-2}Dt)(1 + 4(\gamma s)^{-2}Dt)}$	$\exp(-k_{-1}t)(C_1 + C_2\exp(-D\theta^2 t))/(C_1 + C_2)$
$k_b \ll k_f \;\; (f \approx 0)$ and $\;\; k_f \ll k_{-1}$	$\exp(-k_b t)/\sqrt{(1 + 4s^{-2}Dt)(1 + 4(\gamma s)^{-2}Dt)}$	$\exp(-k_b t)(C_1 + C_2\exp(-D\theta^2 t))/(C_1 + C_2)$

Limiting cases for reaction limited $G(t)$ and $G(\theta, t)$ in a bivalent system, examined with Gaussian and periodic intensity profiles. $G(t)$ is derived from Eqs. 2.2, 5.1, and 5.10–5.12, for shallow bleaching depths ($\eta \ll 1$). $G(\theta, t)$ is derived from Eq. 5.3, and 5.10–5.12, for all bleaching depths.

so that (Eq. 2.3)

$$H(\mathbf{q}, t) = g\exp(-\alpha_1 t) + (1 - g)\exp(-\alpha_2 t) \qquad (5.10)$$

where

$$\alpha_{1,2} = \tfrac{1}{2}(\rho + D_U q^2 + D_V q^2) \qquad (5.11)$$

$$\pm \tfrac{1}{2}\sqrt{(\rho + D_U q^2 - D_V q^2)^2 - 4k_b(k_{-1} + D_U q^2 - D_V q^2)}$$

$$g = \frac{fk_{-1} + fD_U q^2 + (1 - f)D_V q^2 - \alpha_2}{\alpha_1 - \alpha_2}. \qquad (5.12)$$

Eq. 5.3 in conjunction with Eqs. 5.10–5.12 has been previ-

ously derived in the limit where $D_U = D_V$ (Huang, Pearce, and Thompson, manuscript in preparation). Eqs. 5.11 and 5.12 reduce to Eqs. 4.12–4.14 when $q^2 = 0$. Of special interest is the case in which the diffusion coefficient of the two bound species are equal ($D_U = D_V \equiv D$). Here, for an evanescent interference pattern, $H(\theta, t)$ (Eq. 5.10 with $q = \theta$) is given by the product of the right hand side of Eq. 4.11 (with Eqs. 4.12–4.14) and $\exp(-D\theta^2 t)$ and $G(t)$ is given by Eq. 5.3. For a Gaussian-shaped evanescent intensity and shallow bleaching, $G(t)$ is given by the product of the right hand side of Eq. 4.11 (with Eqs. 4.12–4.14) and $[(1 + 4Ds^{-2}t) \cdot (1 + 4D\gamma^{-2}s^{-2}t)]^{-1/2}$.

The shapes of $G(t)$ at the reaction limit for limiting cases are shown in Table 1 for both Gaussian intensity profiles and
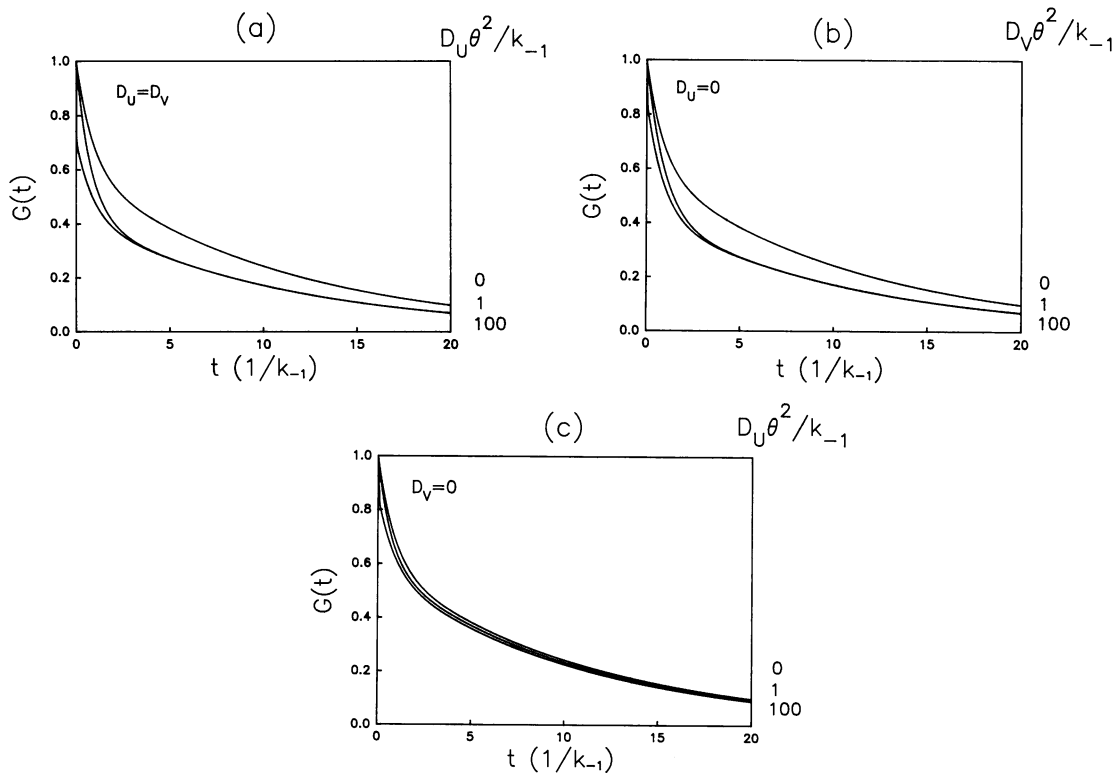
FIGURE 8 $G(t)$ for evanescent interference patterns with variable periods at the reaction limit. $G(t)$ has been calculated from Eqs. 5.3 and Eqs. 5.10–5.12 with (a) $D_U\theta^2 = D_V\theta^2$; (b) $D_U\theta^2 = 0$; or (c) $D_V\theta^2 = 0$. The visibility $\Lambda = 1$ is equal to its maximum value, the bleaching parameter $\eta = 0.75$, and the reaction rates k_{-1}, k_f, and k_b are fixed so that $k_b/k_{-1} = k_f/k_{-1} = 0.1$. As the evanescent period P increases (and the spatial periodicity θ decreases), $G(t)$ approaches a limit in which the recovery is due only to surface kinetics. Conversely, when P decreases and θ increases, $G(t)$ approaches a limit in which the recovery is due only to surface diffusion. If U and V do not diffuse, $G(t)$ does not change with θ. If only one of the two complexes diffuses, with all other conditions equivalent, $G(t)$ decays much faster when V diffuses (b) than when U diffuses (c).

the periodic interference pattern. The shapes of $G(t)$ for evanescent intensity patterns are illustrated in Fig. 8.

DATA ANALYSIS

Equilibrium binding measurements

This paper addresses the measurement of surface binding kinetics using TIR-FPR, for bivalent molecules at membrane surfaces. In particular, two surface binding mechanisms are considered, mechanism I (Fig. 1 a) and mechanism II (Fig. 1 b). Experimentally, one may measure the evanescently excited fluorescence (which is proportional to the surface density of bound molecules, $U_{eq} + V_{eq}$), as a function of the solution concentration A_{eq}. These data will give an absolute (if the fluorescence is calibrated) or relative (if the fluorescence is not calibrated) measure of the surface site density N. Referring to Eq. 1.2, one sees that, for mechanism I, this curve will yield a measure of the apparent association constant K_a (Eq. 1.3), but that these equilibrium measurements will not provide an independent measure of K_1 and K_2. For mechanism II, equilibrium binding curves will yield independent measures of K_1 and K_3N (Eq. 1.4).

Kinetic measurements at large observation areas

TIR-FPR recovery curves have the simplest theoretical shapes when the observation area is large enough so that surface diffusion and solution diffusion parallel to the surface do not affect the measurements. Experimentally, one may confirm that the illuminated area is large enough for the more simple theoretical expressions to be applicable by confirming that the shape of the recovery curve does not change when the size of the illuminated area is changed. In this case, the shape of the recovery curve is given by Eq. 4.4 and depends on four rates: k_{-1}; $k_f = k_2$ (mechanism I) or $k_f = k_3B_{eq}$ (mechanism II); $k_b = k_{-2}$ (mechanism I) or $k_b = k_{-3}$ (mechanism II); and R, which is given in Eq. 3.4 for mechanism I and in Eq. 3.5 for mechanism II. TIR-FPR recovery curves using a large observation area should give information about these rates.

One may first obtain a set of TIR-FPR recovery curves using a large observation area and as a function of the solution concentration A_{eq}. For monovalent binding, the measured recovery rate, k_{obs}, defined as the inverse of the time for which $G(t) = e^{-1}$, increases with the solution concentration A_{eq} until k_{obs} reaches a constant value equal to the membrane dissociation rate k_{-1} (Fig. 9). For bivalent binding, k_{obs} also increases with the solution concentration A_{eq} until it reaches a reaction-limited value. This rate, denoted by k_{rx}, is the inverse of the time for which $G(t) = e^{-1}$, where $G(t)$ is given by Eqs. 4.11–4.14 (Figs. 10 and 11). For mechanism I, k_{rx} is a constant that depends on k_{-1}, $k_f = k_2$, and $k_b = k_{-2}$. For mechanism II, k_{rx} depends not only on the constants k_{-1} and $k_b = k_{-3}$ but also on $k_f = k_3B_{eq}$, which is a function of K_3N and K_1A_{eq} (Eq. 3.1); however, at very high concentrations, the surface becomes saturated with monovalently bound complexes and $k_{rx} \approx k_{-1}$.
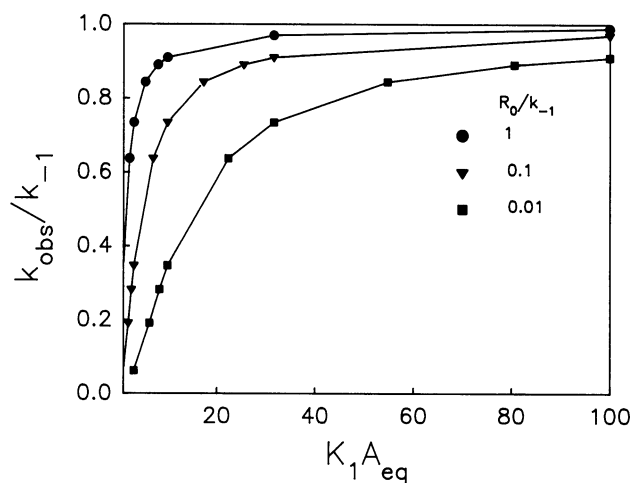

FIGURE 9 Dependence of k_{obs} on the solution concentration for monovalent binding and a large observation area. As the solution concentration A_{eq} is increased, the value of the diffusion rate R increases and the measured rate, k_{obs}, approaches the true membrane dissociation rate, k_{-1}. Curves were calculated numerically using Eqs. 4.6 and 4.7 and are for $R_0/k_{-1} = 1$ (*circles*), 0.1 (*triangles*), and 0.01 (*squares*).

To measure k_{-1} for monovalent binding, one may examine the recovery rates for a set of TIR-FPR recovery curves that have been measured as a function of the solution concentration A_{eq} for the region in which the data do not change with an increase in A_{eq}. These curves are reaction-limited and will report the true membrane dissociation rate k_{-1}. The membrane association rate k_1 may then be obtained from the measured value of the equilibrium association constant K_1 and the measured value of k_{-1}. Alternatively, if K_1, D_A, and N are known, one may curve-fit any TIR-FPR curve to Eq. 4.6 with R as a fixed parameter and k_{-1} as a free parameter.

For bivalent binding according to mechanism I, the same analysis may be applied, except that the reaction-limited curves will be, in general, biexponential. For the reaction-limited concentrations of A_{eq}, one may use the following procedures to obtain values of k_1, k_{-1}, $k_f = k_2$ and $k_b = k_{-2}$:
1) The value of the apparent equilibrium association constant K_a is obtained from an equilibrium binding curve (Eqs. 1.2 and 1.3). 2) The values of the two rates, α_1 and α_2, and the fractional amplitude of the first rate, g, may be obtained from reaction-limited TIR-FPR recovery curves (Eq. 4.11). 3) The value of ρ is found as the sum of α_1 and α_2 (Eq. 4.12). 4) The value of k_{-1} is found by using the following expression

$$k_{-1} = \rho - \frac{\alpha_1(\rho - \alpha_1)}{g\alpha_1 + (1 - g)\alpha_2} \qquad (6.1)$$

which follows from Eqs. 4.12–4.14. 5) The values of $k_b = k_{-2}$ and $k_f = k_2$ are found by sequentially inverting Eqs. 4.12 and 4.13. 6) The values of k_1 and K_2 are found from Eq. 1.1.

For bivalent binding according to mechanism II, the behavior is more complex; even when the concentration A_{eq} is high enough for the TIR-FPR recovery curves to be reaction-limited, $k_{obs} = k_{rx}$ can still change with A_{eq} because of the dependence of k_f on A_{eq}. For this mechanism, the six-step
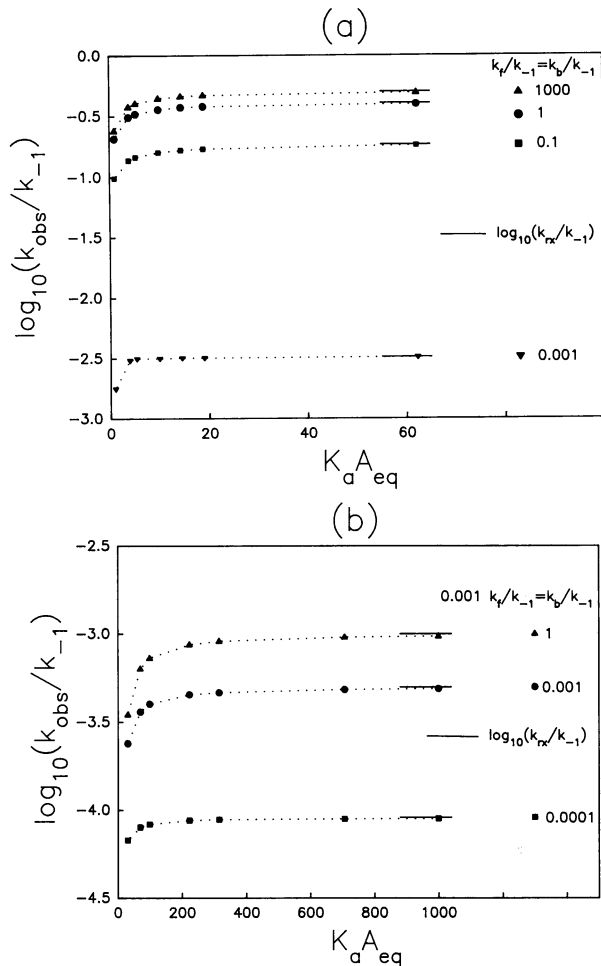
FIGURE 10 Dependence of k_{obs} on the solution concentration for bivalent binding by mechanism I and a large observation area. As the solution concentration A_{eq} is increased, the value of the diffusion rate R increases, and the measured rate, k_{obs}, approaches the reaction-limited value, k_{rx}. K_a, R_0, and R are defined in Eqs. 1.3, 3.3, and 3.4, respectively. The values of k_{obs} and k_{rx} were calculated numerically, with $R_0 = k_{-1}$, using Eqs. 4.1–4.4 or Eqs. 4.11–4.14, respectively. When $k_f \ll k_b$, most of the molecules are in the initial state of attachment and the system behaves as though only monovalent binding occurs (see Fig. 9). (a) Equal quantities of both membrane-bound states are present ($k_f = k_b$). (b) Most of the surface-bound molecules are in the second state of membrane attachment ($k_f = 1000$ k_b).

procedure outlined above for mechanism I may be applied to recovery curves obtained for different solution concentrations A_{eq}. The reaction-limited conditions will correspond to values of A_{eq} for which the obtained values of k_1, k_{-1}, and k_b do not change with A_{eq} and for which $k_f = k_3 B_{eq}$ changes with A_{eq} according to Eq. 3.1.

If reaction-limited data for a large observation area are available for at least two solution concentrations, A_{eq1} and A_{eq2}, then one may distinguish between the two types of bivalent surface-binding mechanisms in that $k_f(A_{eq1}) = k_f(A_{eq2})$ in mechanism I and $k_f(A_{eq1}) \neq k_f(A_{eq2})$ in mechanism II.

Measuring surface diffusion rates

As shown above, the TIR-FPR recovery curve depends in general on seven characteristic rates (k_{-1}, k_f, k_b, R, D_A/ℓ^2,
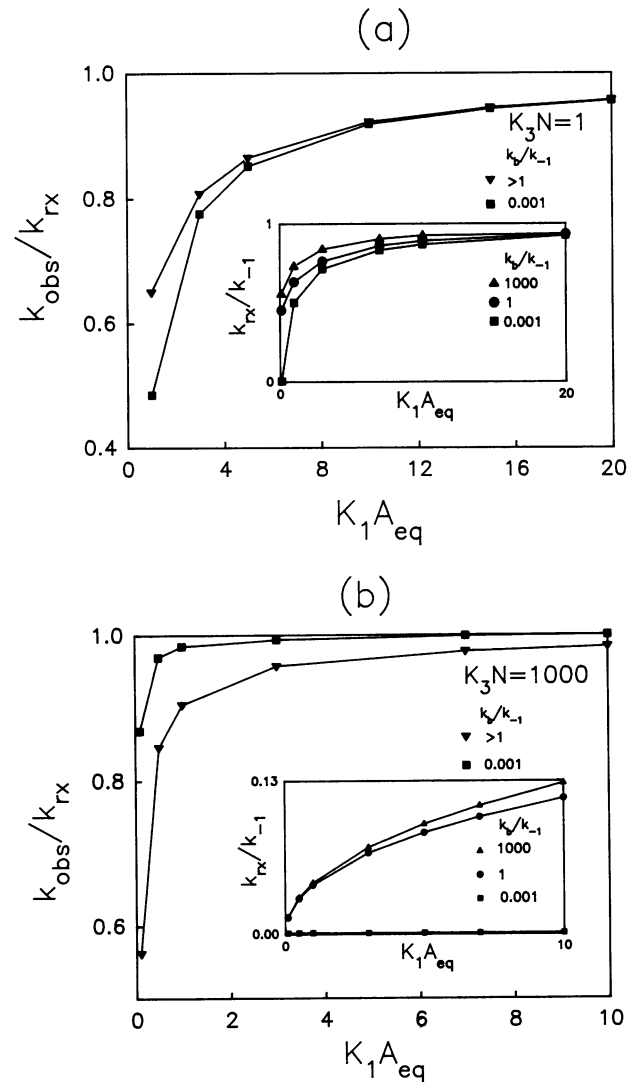

FIGURE 11   Dependence of k_{obs} on the solution concentration for bivalent binding by mechanism II and a large observation area. As the solution concentration A_{eq} is increased, the value of the diffusion rate R increases, and the measured rate, k_{obs}, approaches the reaction-limited value, k_{rx}. R_0 and R are defined in Eqs. 3.3 and 3.5, respectively. The values of k_{obs} and k_{rx} were calculated numerically, with $R_0 = k_{-1}$, using Eqs. 4.1–4.4 or Eqs. 4.11–4.14, respectively. As seen in the insets, k_{rx} approaches k_{-1} as $K_1 A_{eq}$ increases. For given values of $K_1 A_{eq}$ and $K_3 N$, the rate k_f (relative to k_{-1}) was determined using Eqs. 2.6 and 3.1, with $k_3 N/k_{-1} = (K_3 N)(k_b/k_{-1})$. When $K_3 N \ll 1$, most of the molecules are in the initial state of attachment (see Fig. 9). For these plots, (a) $K_3 N = 1$ and (b) $K_3 N = 10^3$.

D_U/ℓ^2, and D_V/ℓ^2, where $\ell = s$ or $\ell = 2\pi/\theta$). The surface diffusion coefficients D_U and D_V are most easily measured when the system is reaction-limited, and the recovery curve depends on only five of these rates (k_{-1}, k_f, k_b, D_U/ℓ^2 and D_V/ℓ^2). If the rates k_{-1}, k_f and k_b have been previously determined by measurements at large observation areas, then recovery curves obtained with evanescent interference patterns and small periods may be curve-fit to Eqs. 5.3 and Eqs. 5.10–5.12 with the three kinetic rates and θ as fixed constants and with D_U and D_V as free parameters. The surface diffusion coefficients D_U and D_V might also be found from recovery curves that are not reaction-limited by determining and fixing D_A and R. The solution diffusion coefficient is

usually known; R may be determined from measurements for large observation areas and low solution concentrations (Eq. 4.9).

SUMMARY

The shapes of TIR-FPR recovery curves have been derived for two mechanisms by which a bivalent molecule may bind to a planar surface. The theoretical approach is a generalization of the previously developed method for monovalent binding (Thompson et al., 1981). The results show that the rate and shape of the recovery curves depend in general on four kinetic rates and three transport rates. For evanescent interference patterns, the general solution for the recovery curve is a sum of five terms that contain complementary error functions. For Gaussian-shaped interference patterns, the general solution is an integral over the product of the five-term summation and the intensity profile. Conditions for which the recovery curves are reaction-limited and report information about the intrinsic surface dissociation kinetics have been defined. Methods for retrieving the intrinsic kinetic rate constants and for distinguishing between different binding mechanisms have been outlined. In addition, the use of this type of experiment to measure the surface diffusion coefficient(s) of the weakly bound molecules has been described. This theory will be applicable primarily to the characterization of weak interactions between protein ligands and substrate-supported planar membranes.

APPENDIX

Derivation of general expression for $G(t)$

For many experimental conditions, the fluorescence arising from molecules in solution which are within the finite depth of the evanescent field but not bound to the surface is negligible, and the fluorescence collection efficiency is equivalent for all adsorbed species. In this case, the fluorescence $F(t)$ is

$$F(t) = Q \int I(\mathbf{r})[U_u(\mathbf{r}, t) + V_u(\mathbf{r}, t)] \, d^2r, \qquad (A1)$$

where Q is the product of the efficiencies of excitation light absorption and fluorescence emission and detection; the integral is over all two-dimensional space; $I(\mathbf{r})$ is the spatial intensity profile of the evanescent field in the sample plane; the subscript u denotes unbleached; and t is the time that has elapsed from the midpoint of the duration of the bleaching pulse. Also, $\mathbf{r} = (x, y)$ is the position in the sample plane, and the spatial origin is defined as the center of the surface area illuminated by the totally internally reflected laser beam. The fluorescence intensities before the bleaching pulse, $F(-)$, immediately after the bleaching pulse, $F(0)$, and after an infinite time, $F(\infty)$, are found from Eq. A1 by replacing U_u and V_u with U_{eq} and V_{eq}, and $[U_u(\mathbf{r}, t)]_{t \to 0, \infty}$ and $[V_u(\mathbf{r}, t)]_{t \to 0, \infty}$, respectively. These definitions of $F(-)$, $F(0)$, and $F(\infty)$, with Eq. A1 and Eq. 2.1 may be used to

write $G(t)$ as

$$G(t) = \frac{\int I(\mathbf{r})[U_b(\mathbf{r}, t) + V_b(\mathbf{r}, t)] \, d^2r}{\int I(\mathbf{r})[U_b(\mathbf{r}, t) + V_b(\mathbf{r}, t)]_{t \to 0} \, d^2r} \qquad (A2)$$

$$U_b(\mathbf{r}, t) = U_{eq} - U_u(\mathbf{r}, t)$$
$$V_b(\mathbf{r}, t) = V_{eq} - V_u(\mathbf{r}, t) \qquad (A3)$$

where the subscript b denotes the surface density of the bleached species.

Differential equations

There are three differential equations that describe the spatial and temporal dependence of the concentrations shown in the surface binding mechanisms of Fig. 2. The solutions to these equations for bleached fluorescent molecules are used to calculate $G(t)$ in terms of the kinetic rate constants, the solution and surface diffusion coefficients, and the experimental conditions. Although bleached, surface-bound molecules exchange with unbleached molecules from solution, the free binding site density remains constant at the equilibrium value (Thompson et al., 1981). Thus, because $B(\mathbf{r}, t) = B$ is a constant, one can define two general constants, k_f and k_b (see text Eq. 2.6) so that the mathematical formalisms for both models of bivalent surface attachment are equivalent.

The solution concentrations of bleached and unbleached molecules are denoted by $A_b(\mathbf{r}, z, t)$ and $A_u(\mathbf{r}, z, t)$, respectively, where z is the position in solution relative to the sample plane. Changes in $A_b(\mathbf{r}, z, t)$, $U_b(\mathbf{r}, t)$, and $V_b(\mathbf{r}, t)$ arise from diffusion in solution, complex formation/dissociation, and surface diffusion. The three coupled differential equations for these functions are

$$\frac{\partial}{\partial t} A_b(\mathbf{r}, z, t) = D_A \nabla_{r,z}^2 A_b(\mathbf{r}, z, t) \qquad (A4)$$

$$\frac{\partial}{\partial t} U_b(\mathbf{r}, t) = k_1 B[A_b(\mathbf{r}, z, t)]_{z \to 0} \qquad (A5)$$

$$+ [D_U \nabla_r^2 - (k_{-1} + k_f)]U_b(\mathbf{r}, t) + k_b V_b(\mathbf{r}, t)$$

$$\frac{\partial}{\partial t} V_b(\mathbf{r}, t) = k_f U_b(\mathbf{r}, t) + [D_V \nabla_r^2 - k_b]V_b(\mathbf{r}, t) \qquad (A6)$$

where D_A is the diffusion coefficient of A in solution, and D_U and D_V are the diffusion coefficients of U and V on the surface. These differential equations describe the surface binding mechanisms for both binding models, without specific reference to a given experimental technique.

Boundary and initial conditions

The difference in the number of adsorptions and desorptions per area per time is the net flux of molecules to the surface. Thus, using Fick's first law, one may write

$$D_A \frac{\partial}{\partial z} [A_b(\mathbf{r}, z, t)]_{z \to 0} = k_1 B[A_b(\mathbf{r}, z, t)]_{z \to 0} - k_{-1} U_b(\mathbf{r}, t) \qquad (A7)$$

In addition, $A_b(\mathbf{r}, z, t)$, $U_b(\mathbf{r}, t)$, and $V_b(\mathbf{r}, t)$ far from the bleached region are negligible during photobleaching and subsequent fluorescence recovery, so that

$$[U_b(\mathbf{r}, t)]_{|\mathbf{r}|\to\infty} = [V_b(\mathbf{r}, t)]_{|\mathbf{r}|\to 0} = 0$$
$$[A_b(\mathbf{r}, z, t)]_{|\mathbf{r}|\to\infty} = [A_b(\mathbf{r}, z, t)]_{z\to\infty} = 0 \tag{A8}$$

Immediately after the bleaching pulse, surface-bound, bleached fluorophores have not yet desorbed and

$$[A_b(\mathbf{r}, z, t)]_{t\to 0} = 0 \tag{A9}$$

Assuming that both complexes are bleached with equal efficiency and that the bleaching process follows first-order kinetics, then the initial densities of bleached, surface-bound species are (Axelrod et al., 1976)

$$[U_b(\mathbf{r}, t)]_{t\to 0} = U_{eq}[1 - e^{-\kappa I(\mathbf{r})}] \simeq U_{eq}\kappa I(\mathbf{r}) \quad (\text{small } \kappa)$$
$$[V_b(\mathbf{r}, t)]_{t\to 0} = V_{eq}[1 - e^{-\kappa I(\mathbf{r})}] \simeq V_{eq}\kappa I(\mathbf{r}) \quad (\text{small } \kappa) \tag{A10}$$

where κ is proportional to the bleaching duration, the bleaching power, and the bleaching efficiency, and the approximations hold for shallow bleaching depths.

Solution

Eqs. A4–A7 may be solved by calculating the Fourier transform with respect to the surface position vector ($\mathbf{r}\to\mathbf{q}$) and the Laplace transform with respect to the normal to the surface ($z\to p$) and time ($t\to\omega$). The equations in Laplace and Fourier space are

$$\left[\frac{\omega}{D_A} + q^2 - p^2\right]A_b(\mathbf{q}, p, \omega)$$
$$= -p[A_b(\mathbf{q}, z, \omega)]_{z\to 0} - \left[\frac{\partial}{\partial z}A_b(\mathbf{q}, z, \omega)\right]_{z\to 0} \tag{A11}$$

$$[\omega + D_U q^2 + k_{-1} + k_f]U_b(\mathbf{q}, \omega) - [U_b(\mathbf{q}, t)]_{t\to 0}$$
$$= k_1 B[A_b(\mathbf{q}, z, \omega)]_{z\to 0} + k_b V_b(\mathbf{q}, \omega) \tag{A12}$$

$$[\omega + D_V q^2 + k_b]V_b(\mathbf{q}, \omega) - [V_b(\mathbf{q}, t)]_{t\to 0}$$
$$= k_f U_b(\mathbf{q}, \omega) \tag{A13}$$

$$D_A\left[\frac{\partial}{\partial z}A_b(\mathbf{q}, z, \omega)\right]_{z\to 0}$$
$$= k_1 B[A_b(\mathbf{q}, z, \omega)]_{z\to 0} - k_{-1}U_b(\mathbf{q}, \omega) \tag{A14}$$

In Eqs. A11–A14 and in subsequent discussion, transformations which have been carried out are denoted solely by the variables in parentheses.

Eqs. A11 and A14 may be used to solve for $A_b(\mathbf{q}, p, \omega)$ as a function of $[A(\mathbf{q}, z, \omega)]_{z\to 0}$ and $U_b(\mathbf{q}, \omega)$. By inverse Laplace transforming ($p\to z$) the resultant expression and using the boundary condition for $z\to\infty$ (Eq. A8), one may obtain an expression for $[A_b(\mathbf{q}, z, \omega)]_{z\to 0}$ as a function of $U_b(\mathbf{q}, \omega)$. This equation together with Eqs. A12 and A13 forms a system of three equations that may be used to

calculate $[A_b(\mathbf{q}, z, \omega)]_{z\to 0}$, $U_b(\mathbf{q}, \omega)$, and $V_b(\mathbf{q}, \omega)$ in terms of kinetic and diffusion parameters. The obtained expressions for $U_b(\mathbf{q}, \omega)$ and $V_b(\mathbf{q}, \omega)$ give solutions for $U_b(\mathbf{q}, t) = L^{-1}_{\omega\to t}U_b(\mathbf{q}, \omega)$ and $V_b(\mathbf{q}, t) = L^{-1}_{\omega\to t}V_b(\mathbf{q}, \omega)$. Defining $\alpha = \omega + D_A q^2$, the sum of these solutions is

$$U_b(\mathbf{q}, t) + V_b(\mathbf{q}, t)$$
$$= e^{-D_A q^2 t}[U_b(\mathbf{q}, t) + V_b(\mathbf{q}, t)]_{t\to 0}L^{-1}_{\alpha\to t}\left[\frac{X(q, \alpha)}{Y(q, \alpha)}\right] \tag{A15}$$

where $X(q, \alpha)$ and $Y(q, \alpha)$ are given in the main text (Eqs. 2.4 and 2.5). Using the inverse Fourier transform of Eq. A15 ($\mathbf{q}\to\mathbf{r}$), and Eq. A10 in Eq. A2 gives a general solution for $G(t)$ (Eq. 2.2).

REFERENCES

Abney, J. R., B. A. Scalettar, and N. L. Thompson. 1992. Evanescent interference patterns for fluorescence microscopy. *Biophys. J.* 61: 542–552.

Axelrod, D., D. E. Koppel, J. Schlessinger, E. Elson, and W. W. Webb. 1976. Mobility measurement by analysis of fluorescence photobleaching recovery kinetics. *Biophys. J.* 16:1055–1069.

Berg, H. C., and E. M. Purcell. 1977. Physics of chemoreception. *Biophys. J.* 20:193–219.

Burghardt, T. P., and D. Axelrod. 1981. Total internal reflection/fluorescence photobleaching recovery study of serum albumin adsorption dynamics. *Biophys. J.* 33:455–468.

Burghardt, T. P., and N. L. Thompson. 1984. Evanescent intensity of a focused Gaussian light beam undergoing total internal reflection in a prism. *Optical Eng.* 23:62–67.

Davoust, J., P. F. Devaux, and L. Leger. 1982. Fringe pattern photobleaching, a new method for the measurement of transport coefficients of biological macromolecules. *EMBO J.* 1:1233–1238.

Dembo, M., and B. Goldstein. 1978. Theory of equilibrium binding of symmetric bivalent haptens to cell surface antibody: application to histamine release from basophils. *J. Immunol.* 121:345–353.

Erickson, J., B. Goldstein, D. Holowka, and B. Baird. 1987. The effect of receptor density on the forward rate constant for binding of ligands to cell surface receptors. *Biophys. J.* 52:657–662.

Goldstein, B., R. G. Posner, D. C. Torney, J. Erickson, D. Holowka, and B. Baird. 1989. Competition between solution and cell surface receptors for ligand: dissociation of hapten bound to surface antibody in the presence of solution antibody. *Biophys. J.* 56:955–966.

Hellen, E. H., and D. Axelrod. 1991. Kinetics of epidermal growth factor/receptor binding on cells measured by total internal reflection/fluorescence recovery after photobleaching. *J. Fluorescence.* 1: 113–128.

Kaufman, E. N., and R. K. Jain. 1991. Measurement of mass transport and reaction parameters in bulk solution using photobleaching: reaction limited binding regime. *Biophys. J.* 60:596–610.

Müller, B., H.-G. Zerwes, K. Tangemann, J. Peter, and J. Engel. 1993. Two-step binding mechanism of fibrinogen to $\alpha IIb\beta 3$ integrin reconstituted into planar lipid bilayers. *J. Biol. Chem.* 268:6800–6808.

Ortega, E., Schweitzer-Stenner, R., and Pecht, I. 1991. Kinetics of ligand binding to the type 1 Fcϵ receptor on mast cells. *Biochemistry.* 30: 3473–3483.

Pearce, K. H., R. G. Hiskey, and N. L. Thompson. 1992. Surface binding

kinetics of prothrombin fragment 1 on planar membranes measured by total internal reflection fluorescence microscopy. *Biochemistry*. 31: 5983–5995.

Pearce, K. H., M. Hof, B. R. Lentz, and N. L. Thompson. 1993. Comparison of the membrane binding kinetics of bovine prothrombin and its fragment 1. *J. Biol. Chem.* 268:22984–22991.

Pisarchick, M. L., and N. L. Thompson. 1990. Binding of a monoclonal antibody and its Fab fragment to supported phospholipid monolayers measured by total internal reflection fluorescence microscopy. *Biophys.J.* 58:1235–1249.

Pisarchick, M. L., D. Gesty, and N. L. Thompson. 1992. Binding kinetics of an anti-dinitrophenyl monoclonal Fab on supported phospholipid monolayers measured by total internal reflection with fluorescence photobleaching recovery. *Biophys. J.* 63:215–223.

Schmidt, C. F., R. M. Zimmermann, and H. E. Gaub. 1990. Multilayer adsorption of lysozyme on a hydrophobic substrate. *Biophys. J.* 57: 577–588.

Thompson, N. L., T. P. Burghardt, and D. Axelrod. 1981. Measuring surface dynamics of biomolecules by total internal reflection fluorescence with photobleaching recovery or correlation spectroscopy. *Biophys. J.* 33: 435–454. Erratum, *Biophys. J.* 35:809.

Tilton, R. D., C. R. Robertson, and A. P. Gast. 1990a. Lateral diffusion of bovine serum albumin adsorbed at the solid-liquid interface. *J. Coll. Int. Sci.* 137:192–203.

Tilton, R. D., A. P. Gast, and C. R. Robertson. 1990b. Surface diffusion of interacting proteins: effect of concentration on the lateral mobility of adsorbed bovine serum albumin. *Biophys. J.* 58:1321–1326.

Weis, R. M., K. Balakrishnan, B. A. Smith, and H. M. McConnell. 1982. Stimulation of fluorescence in a small contact region between rat basophil leukemia cells and planar lipid membrane targets by coherent evanescent radiation. *J. Biol. Chem.* 257:6440–6445.

Zimmermann, R. M., C. F. Schmidt, and H. E. Gaub. 1990. Absolute quantities and equilibrium kinetics of macromolecular adsorption measured by fluorescence photobleaching in total internal reflection. *J. Coll. Int. Sci.* 139:268–280.